Modeling Coherent Backscattering Errors in Fiber Optic Gyroscopes for Sources of Arbitrary Line Width

Seth W. Lloyd, Michel J. F. Digonnet, and Shanhui Fan, *Fellow, IEEE*

***Abstract*—We present a new model of the noise and drift induced by coherent backscattering in a fiber optic gyroscope (FOG) interrogated with a light source of arbitrary temporal coherence. This study is critical to understand whether a FOG driven with a laser instead of a broadband source can attain high sensitivity and stability, which would have the overwhelming benefit of improving the FOG scale factor stability by at least ten-fold and would enable the use of FOGs for inertial navigation of aircrafts. Analytical and numerical solutions bring to light two significant new predictions. First, coherent-backscattering noise can be made negligibly small by utilizing a laser with a very narrow linewidth (less than ∼20 kHz), although in this regime the drift is high. Second, by using a laser with a broad linewidth (greater than ∼10 MHz), both the noise and the drift are low enough for aircraft inertial navigation. The dependencies of the noise and drift on fiber loss, loop coupling coefficient, and backscattering coefficient are also presented to define the optimum mode of operation of this new class of FOGs.**

***Index Terms*—Backscattering drift, backscattering noise, coherent backscattering, fiber optic gyroscope, laser phase noise, Sagnac interferometer.**

I. Introduction

INTENSE research efforts throughout the 1980s and early 1990s showed that the three main error sources in a fiber optic gyroscope (FOG), namely Rayleigh backscattering, [1] the Kerr effect, [2] and polarization coupling, [3] all originate from the use of coherent laser light to interrogate the FOG, and that these errors limited the performance of a laser-driven FOG far above inertial-navigation requirements. These errors were subsequently mitigated by replacing the laser with a source of very low coherence. The additional developments of advanced closed-loop signal-processing schemes, polarization-maintaining (PM) fibers, multifunction integrated optical circuits (MIOCs), and special fiber windings to reduce the Shupe effect, led to further performance improvements. The bias drift and angular random walk (ARW) noise of modern FOGs now match or even exceed the performance of competing optical inertial-navigation technologies such as ring laser gyros (RLGs) [4], [5].

The only primary performance metric where modern FOGs continue to lag other technologies is the scale-factor stability. The scale factor is the constant of proportionality that relates the applied rotation rate Ω_R to the Sagnac phase shift ϕ_S induced by a rotation in the FOG's Sagnac interferometer [6]. It is given by $S_F = \phi_S/\Omega_R = 2\pi LD/(\lambda c)$, where L is the loop length, λ is the mean wavelength of the light, and D is the loop diameter. A FOG measures ϕ_S, and the instantaneous rotation rate Ω_R is recovered from this measured value by dividing it by the scale factor. Any error in the knowledge of S_F therefore leads to a commensurate error in Ω_R. For aircraft navigation, the maximum tolerable error in S_F is $\sim$1 part per million (ppm) [6], [7]. The main source of scale-factor error is thermal instability in λ; stabilizing this mean wavelength to the ppm level has proven challenging [8]. As a result, the best FOGs achieve scale-factor stabilities of 10–100 ppm, [4], [5] at least 10 times higher than the 1-ppm scale-factor stability of RLGs, and than the stability requirement for aircraft navigation. Because the inferred rotation rate Ω_R is directly proportional to the source wavelength λ, any improvement in the wavelength stability leads to a directly proportionate improvement in the minimum detectable rotation rate.

A possible method for increasing the scale-factor stability is to replace the broadband source with a 1.5-μm semiconductor laser. Widely used in telecom systems, these lasers are commercially available with a wavelength stability of 1 ppm or better. Furthermore, because telecom lasers exhibit negligible excess noise, they would also remove the excess noise inherent in broadband sources, ultimately lowering the FOG ARW. Because for a given measurement bandwidth (BW) the minimum detectable rotation rate equals $\mathrm{ARW} \bullet \sqrt{\mathrm{BW}}$, reductions in ARW lead to direct improvements in the minimum detectable rotation rate. Finally, the use of a laser would reduce power consumption, complexity, and cost.

The challenge, of course, is overcoming the errors resulting from the use of coherent light, errors which were the very reason for abandoning lasers in FOGs years ago. However, since that time, intervening technological advances have altered the FOG landscape. Improvements in the optical components used in FOGs have led to much lower losses. Lower losses imply reduced circulating power in the sensing fiber and hence significantly reduced Kerr-induced drift. The development of

Manuscript received October 15, 2012; revised February 26, 2013; accepted March 28, 2013. Date of publication May 06, 2013; date of current version May 31, 2013. This work was supported in part by Litton Systems, Inc., a wholly owned subsidiary of Northrop Grumman Corporation.

S. W. Lloyd is with Electrical Engineering, Stanford University, Stanford, CA 94305 USA.

M. J. F. Digonnet is with Ginzton Lab, Stanford University, Stanford, CA 94305 USA (e-mail: silurian@stanford.edu).

S. Fan is with Stanford University, Stanford, CA 94305 USA.

Color versions of one or more of the figures in this paper are available online at http://ieeexplore.ieee.org.

Digital Object Identifier 10.1109/JLT.2013.2261283

improved PM fibers and MIOCs with high-extinction-ratio polarizers diminishes polarization-related errors. Backscattering-induced errors are also expected to be reduced, in part because Rayleigh scattering is much lower at 1.55 μm than at the shorter wavelengths used in early FOGs.

Of these three parasitic effects, we expect backscattering to be the dominant source of error. Unfortunately, while backscattering has been studied in other optical gyroscopes [9], [10], there is no model to predict the magnitude of the noise or drift due to backscattering in an interferometric laser-driven FOG. Cutler published an analysis [1] that was insightful for recognizing the potentially limiting effects of scattering, but it assumed that all scatterers in the fiber loop scattered in phase, leading to a vastly overestimated spurious drift. Cutler's model also did not account for the significant effects of the time-dependent phase modulation typically used to bias a FOG, for source phase noise, and for the symmetry of light scattered in the clockwise (cw) and counter clockwise (ccw) directions. Takada modeled backscattering noise more accurately, but he limited his study to short coherence lengths and did not include phase modulation [11]. Mackintosh *et al.* performed theoretical calculations and presented experimental results that included phase modulation [12]. Importantly, they showed that under certain conditions the use of modulation and of a 50% coupler can significantly reduce the effects of backscattering, but again only in the limit of short coherence lengths. Using a different approach, Krakenes *et al.* developed a more robust model of the effect of laser phase noise on backscattering-induced noise in Sagnac interferometers [13]. This model, however, also assumed a coherence length much shorter than the loop length. In this limit, an increase in noise with increasing coherence length was predicted [12], [13].

This paper reports the development and exploitation of a more thorough theory that expands on earlier work to model the backscattering-induced noise and drift for an arbitrary coherence length in the presence of phase modulation. We first present a brief background of the physics of the noise and drift arising from coherent backscattering in a Sagnac interferometer. We then describe numerical and analytical models that quantify these two errors. We apply these models to a particular laser-driven gyroscope to examine the dependence of noise and drift on coherence length. We predict that by choosing a coherence length either much longer or much shorter than the loop length, the backscattering-induced noise can be reduced well below the excess-noise level of the same FOG driven with a broadband source. We show that in the opposite limit of a moderate coherence length ($\sim$10 m), by selecting appropriate system parameters (namely push-pull phase modulation at the loop proper frequency, a low-loss fiber, and a 50% loop coupler) a laser-driven FOG can exhibit low enough noise and drift to meet navigation-grade requirements. These predictions establish for the first time the path to a FOG with noise, drift, and scale-factor performance that exceeds that of RLGs and other inertial-navigation optical gyros, all in a system that is simpler, cheaper, and more energy-efficient than existing FOGs. Experimental evidence of these predictions will be presented in a separate upcoming journal article.

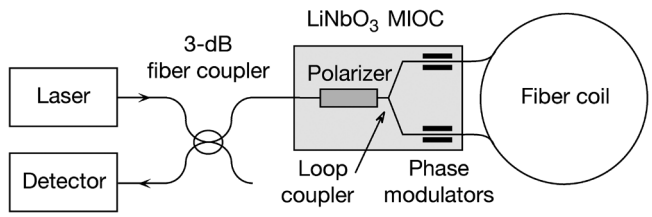

Fig. 1. Diagram of the open-loop laser-driven fiber optic gyroscope.

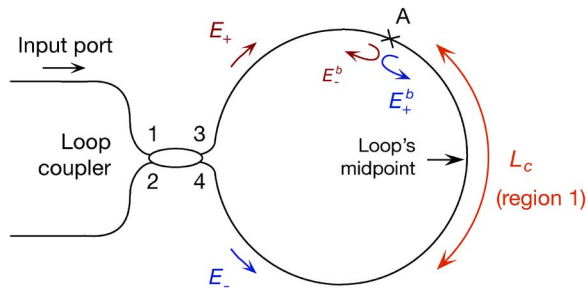

Fig. 2. Effect of backscattering in a Sagnac interferometer.

II. Physics of Backscattering in a FOG

The diagram of the laser-driven FOG is shown in Fig. 1. It consists of the standard minimum-configuration open-loop FOG [6] in which the broadband source has been replaced with a laser. The components are a laser source, a photo detector, an input/output coupler, an in-line polarizer, the loop coupler, one or two phase modulators for biasing, and the fiber coil. One can use all-fiber passive components, or the polarizer, loop coupler, and modulators can be combined on an MIOC, as shown in Fig. 1. Closed-loop signal-processing techniques can also be added. Since operation with a laser is not expected to change the benefits of closed-loop operation, only open-loop operation is considered here.

Interferometric FOGs utilize the well-known Sagnac effect [6]. When two light signals traverse a closed path in opposite directions simultaneously, a rotation about an axis perpendicular to the plane of the path induces a differential phase shift proportional to the rotation rate. This phase shift can be measured in a Sagnac fiber interferometer (Fig. 2), which splits an input light signal into two signals of nominally equal power with a coupler, launches each signal in the loop in opposite directions, then recombines the signals on exit at the coupler. Under zero rotation and in the absence of other nonreciprocal and asymmetric time-dependent effects, the optical paths followed by the two signals are identical resulting in complete destructive interference at port 2 and fully constructive interference at port 1 [6]. Rotation breaks this reciprocity and results in each signal experiencing optical paths that differ by an amount proportional to the rotation rate [6]. Through interference, some of the power then exits at port 2, reducing the power at port 1. The rotation rate is inferred from a measurement of this power change.

The two primary sources of backscattered signal in a fiber are Rayleigh scattering and reflections at splices and terminations. Rayleigh scattering originates from inhomogeneities of random amplitude randomly distributed along the fiber. For time scales

on the order of the loop delay, these two random processes can be considered stationary in time. While reflections at splices and terminations can, in theory, be minimized, Rayleigh scattering is an inherent property of fibers that cannot be avoided.

When the primary cw field E_+ is backscattered at a particular point A (see Fig. 2), a small portion of it, E_-^b, is backscattered in the ccw direction and travels back to the loop coupler, where it adds either coherently or incoherently to the two primary signals E_+ and E_-. The fields E_-^b, E_-, and E_+ have traveled different optical paths (except for the scattering center located at the loop's midpoint). If this difference is smaller than the coherence length L_c of the light, these fields are coherent and interfere. This is true for all scatterers located within $\pm L_c/2$ of the midpoint (region 1, see Fig. 2). The rest of the scatterers produce backscattered fields with a path difference greater than L_c. These fields are incoherent with the primary fields and do not interfere but add in intensity.

This process leads to two deleterious effects. First, because backscattered fields generated in region 1 interfere coherently with the primary fields, and because there is a path imbalance between interfering fields, as with any unbalanced interferometer the interference process converts source phase noise into random fluctuations in the output power. This constitutes a source of noise. Backscattered fields generated outside of region 1, on the other hand, add in intensity leading to considerably weaker and essentially negligible intensity noise. In a FOG, this noise is generally quantified either as a random-walk noise (in $\mathrm{rad}/\sqrt{\mathrm{Hz}}$) when expressed in terms of phase error, or an angle random-walk noise $(\mathrm{deg}/\sqrt{\mathrm{h}})$ when converted to an equivalent rotation-rate error. Importantly, source phase noise, not random variations in the scatterers' phase or location distributions, causes the backscattering-induced noise in a FOG.

The second deleterious effect of backscattering is drift. Because the optical paths traversed by the fields backscattered in the cw and ccw directions are inherently different, backscattering generally produces a non-zero mean signal, i.e., a bias error. This error could be easily compensated if it were constant. However, environmental perturbations of the coil, in particular temperature variations and acoustic noise, cause the bias error to fluctuate. These fluctuations are generally slow compared to the loop delay and give rise to *bias drift*. This drift is indistinguishable from a rotation-induced change and thus constitutes an error. Bias drift is measured in rad when expressed in terms of phase, or in deg/h for a rotation-rate error. Here too the majority of this effect arises from fields backscattered in region 1; the fields backscattered outside of region 1 add in intensity and contribute to negligible drift.

In summary, the only portion of the coil that contributes significantly to backscattering noise and drift is region 1. When interrogating a FOG with light of very long coherence length (e.g., $L_c \approx L$, typically 100–1000 m), this region is as long as can be and all scatterers contribute to coherent noise and drift. As a result, these two sources of error are very large, as observed in early FOGs driven with a laser. On the other hand, when the light has a very short coherence length (typically less than 100 $\mu\mathrm{m}$), region 1 is exceedingly short and both errors are reduced to the point of being negligible [6].

III. Modeling Coherent Backscattering in a FOG

We begin with the same basic field equations used in [11], [13], but considering the FOG configuration of Fig. 1. We assume single-mode operation with a single state of polarization throughout the fiber, thus scalar fields are used. The output field from the fiber loop at port 1 (see Fig. 2) consists of four components, namely the two primary signals E_+ and E_-, and the two backscattered signals E_+^b and E_-^b. Expressing the complex input field at port 1 as $E_0 e^{j[\omega_0 \cdot t + \phi(t)]}$, where ω_0 is the center angular frequency and $\phi(t)$ is the source phase noise, the two primary fields can be written as

$$E_+(t) = a_{13}a_{41}E_0 e^{-\alpha L/2} F_+(t) \tag{1}$$

$$E_-(t) = a_{14}a_{31}E_0 e^{-\alpha L/2} F_-(t) \tag{2}$$

$$F_+(t) = \exp\{j\,[\omega_0.(t - L/v) + \phi(t - L/v) + \phi_s/2 + \Phi_1(t - L/v) + \Phi_2(t)]\} \tag{3}$$

$$F_-(t) = \exp\{j\,[\omega_0.(t - L/v) + \phi(t - L/v) - \phi_s/2 + \Phi_1(t) + \Phi_2(t - L/v)]\} \tag{4}$$

where a_{ij} are the complex coupling coefficients between ports n and m of the loop coupler (the coupler is reciprocal, so $a_{ij} = a_{ji}$), v is the effective phase velocity of the fundamental mode in the fiber, α is the power loss coefficient of the fiber, and $\Phi_1(t)$ and $\Phi_2(t)$ are the phase modulations imparted by the two phase modulators placed in the loop for biasing (when only one modulator is used $\Phi_2(t) = 0$). Similarly, the two total backscattered fields can be expressed as

$$E_+^b(t) = a_{14}a_{41}E_0 F_+^b(t) \tag{5}$$

$$E_-^b(t) = a_{13}a_{31}E_0 F_-^b(t) \tag{6}$$

$$F_+^b(t) = \int_0^L jA^*(L-z)\mathrm{e}^{j[\omega_0.(t-2z/v)+\phi(t-2z/v)+\Phi_2(t)+\Phi_2(t-2z/v)]} \times \mathrm{e}^{-\alpha z}dz \tag{7}$$

$$F_-^b(t) = \int_0^L jA(z)\mathrm{e}^{j[\omega_0.(t-2z/v)+\phi(t-2z/v)+\Phi_1(t)+\Phi_1(t-2z/v)]} \times \mathrm{e}^{-\alpha z}dz \tag{8}$$

where $A(z)$ is a random variable representing the scattering coefficient at position z. Rayleigh backscattered light suffers a $\pi/2$ phase shift relative to the incident field, [11], [13] which explains the factor of j in (7) and (8). These equations do not include a Sagnac phase shift, an approximation valid in the limit of even fairly large rotation rates.

A. Complex Scattering Coefficient

Equations (7) and (8) contain important differences from earlier formulations. In [13], each backscattering coefficient was assumed to have a real random amplitude and a fixed phase relative to the incident light of $\pi/2$. However, in investigations

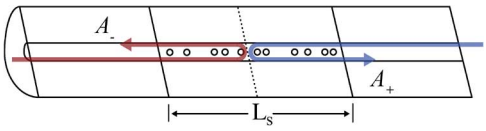

Fig. 3. Distributed scatterers along segment L_s of the sensing fiber.

dealing with general Rayleigh scattering not specific to FOGs, both the scattering amplitude and phase were assumed to be random [14], [15]; the scattering coefficient was therefore represented as a circularly complex Gaussian random variable. This apparent inconsistency in the treatment of the phase appears to be attributable to the scale considered.

When scattering is considered at the microscopic, single-scatterer level, light scattered by Rayleigh scattering is shifted relative to the incident light by a fixed value of $\pi/2$, regardless of the direction of incident light [13]. However, if scattering is considered at the mesoscopic scale, where scattering from a segment of length L_s is taken as the sum of the contributions of the many scatterers along the segment (Fig. 3), then the phase shift is no longer $\pi/2$. Instead, because the scatterers are randomly located along L_s, the complex sum of the fields they scatter results in a complex scattering coefficient with a random phase and amplitude [14], [15]. Because of the fixed $\pi/2$ phase shift of each individual scatterer, these random phases are clustered around a mean value of $\pi/2$. For light incident from the right in Fig. 3, scattering can be represented by the complex scattering coefficient $A_+ = jA$. For light incident from the left, the scatterers are encountered in the *reverse* order. Aside from the $\pi/2$ phase shift, this reversal results in the backscattered light having the same amplitude but the opposite phase. However, because each individual scatterer still also imparts a $\pi/2$ phase shift, the net effect is a scattering coefficient $A_- = jA^*$. This formulation is valid at any scale, with changes in scale being reflected only in the distribution of the complex scattering coefficient A. For further discussion of this issue, refer to [16]. For maximum flexibility, the model presented here assumes complex scattering coefficients.

B. Output Intensity and Backscattering Error

The time-dependent output intensity of the FOG is $I_{out}(t) = |E_+ + E_- + E_+^b + E_-^b|^2$. When using two symmetrically located phase modulators and a standard push-pull modulation scheme ($\Phi_1(t) = -\Phi_2(t) = \Phi(t)$), with the help of (1)–(8) $I_{out}(t)$ becomes

$$\begin{aligned} I_{out}(t) = I_0\Big\{ & 4|a_{14}|^2|a_{13}|^2 e^{-\alpha L}\cos^2[\phi_s/2+\Phi(t-L/v)-\Phi(t)] \\ & + e^{-\alpha L/2}|a_{14}|^2 a_{13}a_{14}^* F_+(t)F_+^{b*}(t) + cc \\ & + e^{-\alpha L/2}|a_{13}|^2 a_{14}a_{13}^* F_+(t)F_-^{b*}(t) + cc \\ & + e^{-\alpha L/2}|a_{14}|^2 a_{13}a_{14}^* F_-(t)F_+^{b*}(t) + cc \\ & + e^{-\alpha L/2}|a_{13}|^2 a_{14}a_{13}^* F_-(t)F_-^{b*}(t) + cc \\ & + a_{14}^2 a_{13}^{*2} F_+^b(t)F_-^{b*}(t) + cc \\ & + |a_{14}|^2\left|F_+^b(t)\right|^2 + |a_{13}|^2\left|F_-^b(t)\right|^2 \Big\} \end{aligned} \tag{9}$$

where I_0 is the intensity incident on the loop coupler and cc represents the complex conjugate of the preceding term. The rotation-rate information is contained in the interference of the primary waves (first term in (9)). The bias error $I_n(t)$ due to backscattering is dominated by the interference of the primary and backscattered fields (second through fifth terms). The sum of these four terms can be simplified to

$$\begin{aligned} \frac{I_n(t)}{I_0 e^{-\alpha L}} = & |a_{14}|^2 a_{13}a_{14}^*\left[F_+(t)+F_-(t)\right]F_+^{b*}(t) + cc \\ & + |a_{13}|^2 a_{14}a_{13}^*\left[F_+(t)+F_-(t)\right]F_-^{b*}(t) + cc \end{aligned} \tag{10}$$

The sixth term in (9) is the interference between the cw and ccw backscattered fields, while the final term is the intensity of each backscattered field. Since the backscattered fields are typically much weaker than the primary fields these last two terms are neglected.

Equation (10) depends on two independent random processes: the temporal fluctuations of the source's phase $\phi(t)$, and the complex scattering coefficient $A(z)$, which is a function of position along the fiber. The time-dependent phase modulation $\Phi(t)$ causes $I_n(t)$ to be a non-stationary random process.

Equation (10) represents the total backscattering-induced error. Because the FOG output is measured with a synchronous-detection system, the noise that is actually measured is only the portion of this bias error that falls within the finite bandwidth of the detection system, centered on the modulation frequency f_m. Thus the expected value $I_n(t)$ ((10)) at f_m represents the bias error, while the standard deviation of $I_n(t)$ after filtering around f_m represents the noise.

As explained previously, the bias error is not stationary, due to time-varying external perturbations of the coil. These temporal perturbations change the relative phases of individual scattered fields, since fields scattered at different points encounter the perturbation at different times. This changes the magnitude and phase of the complex sum of these individual scattered fields, i.e., of the total scattered fields $E_+^b(t)$ and $E_-^b(t)$. A brute-force calculation of the effect of such a perturbation could, of course, be carried out. However, the problem could no longer be treated as a linear time-invariant system because of the time-varying nature of the perturbation. This would significantly increase the complexity of the simulations. Alternatively, the standard deviation of the expected bias error across all possible distributions of scatterers can serve as an upper bound on the expected drift. The rationale is that this standard deviation gives a measure of the expected change in the bias error as the magnitude and position of the scatterers are changed, while a time-varying perturbation is expected to change only the phase of the scatterers, which is equivalent to changing only their position. The standard deviation is therefore expected to overestimate the bias drift. This is the approach used in this work to estimate an upper bound value of the bias drift. The standard deviation was calculated from the power spectral density of $I_n(t)$. It should be noted that the symmetric windings of the sensing coil used to minimize the effect of such thermal perturbations on the primary fields [17] will not necessarily reduce the bias drift induced by backscattering because the latter does not occur symmetrically about the loop midpoint.

C. Statistics of Backscattering and Source Phase Noise

Calculating the power spectral density of $I_n(t)$ ((10)) requires knowledge of the statistics of the backscattering coefficient $A(z)$ and of the source phase noise $\phi(t)$. For a statistically homogeneous medium such as the glass in optical fibers, and for the length scales under consideration ($z - z' \gg \lambda_0$), the autocorrelation of the Rayleigh scattering process is [15]

$$\langle A^*(z')(A(z)\rangle = \alpha_B \delta(z - z') \tag{11}$$

where α_B is the fiber's Rayleigh backscattering coefficient, which depends on the Rayleigh scattering coefficient of the material and on the fiber recapture factor.

The source phase noise is assumed to follow a Wiener-Levy process with stationary independent increments. As such, the statistical distribution of the phase difference between any two points in time along the laser signal depends only on the temporal delay between these two points. This phase difference $\Delta\tilde{\phi}(t,\tau) = \phi(t+\tau) - \phi(t)$ is then described by the probability density function [18]

$$P\left(\Delta\tilde{\phi}(t,\tau)\right) = \frac{\exp\left(-\Delta\tilde{\phi}^2(t,\tau)/2\sigma^2(\tau)\right)}{\sqrt{2\pi}\sigma(\tau)} \tag{12}$$

where $\sigma^2(\tau) = 2\pi\Delta f|\tau|$. This probability function depends only on Δf, the full width at half-maximum of the source frequency spectrum linewidth. Furthermore, the phase changes over two non-overlapping time intervals $\Delta\tilde{\phi}_1(t_1,\tau_1)$ and $\Delta\tilde{\phi}_2(t_2,\tau_2)$ are statistically independent [18].

D. Numerical Simulation Method

The power spectral density of (10) can be calculated numerically. To simplify this calculation, it is useful to rewrite (7) and (8) using the substitution $\tau = 2z/v$, which gives

$$\begin{aligned} F_+^b(t) &= \frac{v}{2}\int_{-\infty}^{\infty} A\left(L-\frac{v}{2}\tau\right) e^{j[\omega_0\cdot(t-\tau)+\phi(t-\tau)+\Phi_2(t)+\Phi_2(t-\tau)]} \\ &\quad \times e^{-\frac{v\alpha}{2}\tau} d\tau \\ &= \frac{v}{2} e^{j\Phi_2(t)}\cdot[A_1(t) * B_1(t)] \end{aligned} \tag{13}$$

$$\begin{aligned} F_-^b(t) &= \frac{v}{2}\int_{-\infty}^{\infty} A\left(\frac{v}{2}\tau\right) e^{j[\omega_0\cdot(t-\tau)+\phi(t-\tau)+\Phi_1(t)+\Phi_1(t-\tau)]} \\ &\quad \times e^{-\frac{v\alpha}{2}\tau} d\tau \\ &= \frac{v}{2} e^{j\Phi_1(t)}\cdot[A_2(t) * B_2(t)] \end{aligned} \tag{14}$$

where

$$A_1(t) = \left\{ \begin{array}{cc} A\left(L-\frac{v}{2}t\right) e^{-\frac{v\alpha}{2}t} & 0 < t < \frac{2L}{v} \\ 0 & \text{otherwise} \end{array} \right\} \tag{15}$$

$$A_2(t) = \left\{ \begin{array}{cc} A\left(\frac{v}{2}t\right) e^{-\frac{v\alpha}{2}t} & 0 < t < \frac{2L}{v} \\ 0 & \text{otherwise} \end{array} \right\} \tag{16}$$

$$B_1(t) = \exp\{j[\omega_0 t + \phi(t) + \Phi_1(t)]\} \tag{17}$$

$$B_2(t) = \exp\{j[\omega_0 t + \phi(t) + \Phi_2(t)]\} \tag{18}$$

The interpretation of (13) and (14) is fairly intuitive. The fiber acts as a linear system with an impulse response dictated by the complex amplitude of the scatterer at point z and by the round-trip propagation time and loss between the input to the loop and the scatterer. The output of the system is the convolution of the input (the phase-modulated light) with the impulse response, remembering to include the additional phase modulation that occurs as the light exits the Sagnac loop. Expressing the backscattered fields as a convolution simplifies the numerical calculations and allows the fields to be calculated more efficiently using a fast Fourier transform algorithm.

The backscattering-induced errors can be calculated in a fairly straightforward manner by an iterative process. A sample function of the source phase noise is first generated at N time-sample points by using a random number generator and applying the known Gaussian statistics of the source's phase ((12)) and the independent increments property. A single sample function of the scatterers $A(z)$ is also generated at M spatial-sample points using the known statistical properties of $A(z)$ ((11)). Note that the convolutions in (13) and (14) place a constraint on the spatial sampling used, namely $\Delta z = v\Delta t/2$. For these two sample functions, the output intensity $I_n(t)$ is calculated using (10) and (13)–(18). The power spectral density is calculated as the modulus squared of the Fourier transform of $I_n(t)$. The process is then repeated for different sample functions of $A(z)$ (each of these samples representing a fiber with the same scattering coefficient α_B) and of $\phi(t)$ (each of these samples representing a source with the same linewidth). The results of hundreds of such iterations are then averaged to obtain the final result.

The convergence of this iterative process was determined heuristically along three parameters. First, the number of time samples N was increased until increasing the time duration of the simulation further led to less than 1% change in the predicted bias error. Second, M was increased (or equivalently Δz decreased) until a similar convergence was observed. Third, N was again varied to ensure that adjusting M had not altered the convergence of N. Finally, once both N and M were fixed, the expected bias error was calculated repeatedly for different sample functions of the source phase and of the fiber scattering distribution, of lengths N and M, respectively. The average of the predicted bias error over these distributions was then calculated, and the process was again repeated until changes in the average with additional iterations were again below 1%. This resulted in an estimate of the upper bound of the bias error. The noise was observed to converge much more rapidly than the bias error, thus the same process also yielded a reliable estimate of the backscattering-induced noise.

E. Analytical Solution

The numerical simulation method of Section III-D allows maximum flexibility by making a minimum number of assumptions about the system. However, iterating over many sample functions of $A(z)$ and $\phi(t)$ can quickly become computationally intensive. To reduce the computation time, starting from (10)–(13) we showed that for the important particular case of the sinusoidal phase modulation typically used to bias an open-loop FOG, it is possible to derive a direct analytic solution for the autocorrelation $R_n(\tau)$ of $I_n(t)$. Specifically, this phase modulation is $\Phi(t) = \phi_m \cos(2\pi f_m t)$, where ϕ_m is the modulation depth and $f_m = v/(2L)$ is the loop proper frequency [6]. The

TABLE I
PARAMETERS OF THE FOG MODELED IN THIS WORK

FOG parameters	Value
Fiber length L	150 m
Modulation index ϕ_m	0.46 rad
Effective index of fiber mode	1.468
Propagation loss coefficient α	1.15 dB/km
Coupling coefficient of loop coupler κ	0.5

derivation is straightforward but lengthy, and the final expression occupies about a page, so it is not reproduced here. It can be found in [16]. This expression is a sum of two terms, each one an infinite series of products of Bessel functions and various sinusoids of the general form

$$4\alpha_B e^{-\alpha L} g(\kappa) \times \int_0^L e^{-2\alpha z} e^{-\pi\Delta f\left(2|\tau|+2\left|\frac{2z-L}{v}\right|-\left|\tau+\frac{2z-L}{v}\right|-\left|\tau-\frac{2z-L}{v}\right|\right)} \cdot \cos(2\pi f_m \tau) \times \left(J_0\left(A_1\cos\left(\frac{\pi z}{L}\right)\right)\left(J_0(A_1)+J_0(A_2)\right)\right) dz \quad (19)$$

where $\kappa = |a_{13}|^2|a_{14}|^2$ is the power coupling coefficient of the loop coupler, $A_1 = 4f_m \sin(\pi f_m \tau)$, $A_2 = 4f_m \cos(\pi f_m \tau)$, and $g(\kappa)$ is a polynomial in κ. The integrals in (19) are evaluated numerically for given FOG parameters. Equation (19) represents a time average of the autocorrelation of $I_n(t)$. Calculating numerically the Fourier transform of $R_n(\tau)$ thus yields the desired power spectral density, from which the expected bias error and noise at f_m can be extracted. These numerical calculations yield direct results without any need for averaging over multiple sample functions as in the numerical simulation, which reduces computation time in many instances by more than two orders of magnitude.

IV. MODEL RESULTS

Both the numerical method and the analytic solution are powerful tools to fully model the effects of backscattering in a FOG. They were first used to model identical gyroscopes and verify that they produced the same solutions, which added confidence to the accuracy of the results. In addition, the numerical model allows a broad exploration of the entire backscattering parameter space. It is straightforward, for example, to set $\Phi_2(t) = 0$ and consider how a configuration utilizing a single phase modulator instead of a push-pull phase modulator affects the backscattering-induced errors. This model can therefore be used to optimize the performance of a FOG in the presence of backscattering in order to achieve different performance metrics for a variety of applications.

The four parameters of primary interest are the source coherence, the backscattering coefficient, the loop length, and the coupling coefficient. These parameters are discussed individually in this section. In these calculations, unless otherwise specified we modeled a FOG with the parameters of an experimental gyroscope that we assembled in our laboratory (see Table I). The modulation index was selected to maximize the output signal.

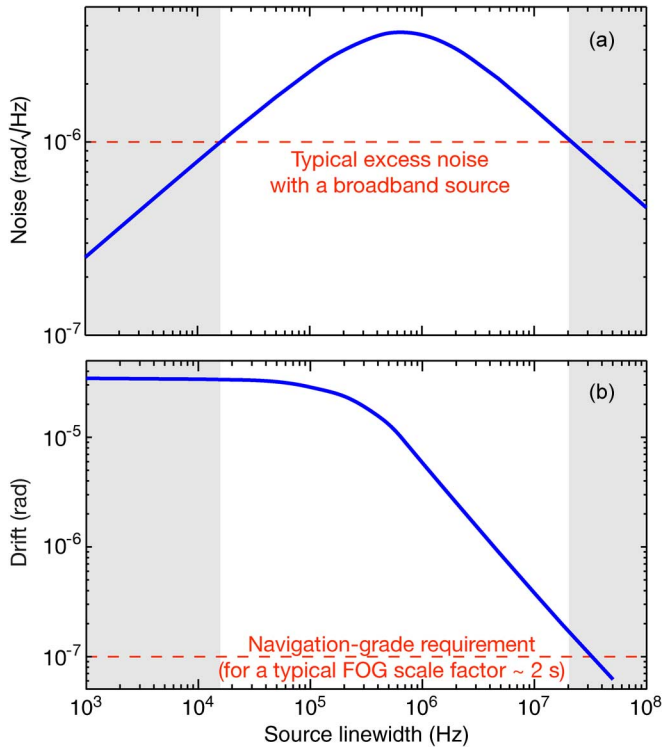

Fig. 4. (a) Angular random walk and (b) bias error calculated for the laser-driven FOG of Fig. 1 with the parameter values of Table I.

A. Source Coherence

Fig. 4(a) shows the predicted FOG random walk noise as a function of the source linewidth Δf. The dependence shows several important characteristics. As the coherence length is initially increased, the noise increases. This makes intuitive sense because as explained earlier, coherently backscattered photons arise from a segment of fiber centered on the loop midpoint and with a length L_c. Thus as L_c increases, the number of coherent scatterers increases, leading to higher noise. When the coherence length reaches the loop length ($L_c = L$), all the scatterers present in the loop contribute to the coherent interference, hence increasing the coherence length further no longer adds more scatterers and the noise stops increasing. When the coherence length is increased further ($L_c > L$), the source phase noise decreases, which leads to diminishing fluctuations in the phase of the backscattered signals, and hence reduced noise. A significant finding of this work is that the backscattering noise can be reduced by increasing the coherence length beyond the loop length.

Fig. 4(b) shows the predicted dependence of the bias error on the linewidth. For the same reasons as the noise, the bias error initially increases with increasing coherence length. Once L_c exceeds the loop length, however, the bias error flattens out and is essentially independent of the coherence length. The reason is also that all scattered photons then interfere coherently with the primary photons. Therefore, as the coherence length is increased beyond the loop length, the mean error is already maximum and no longer increases.

Fig. 4 also make significant predictions regarding the absolute values of the noise and bias drift. First, even at its maximum

value (when $L_c = L$) the random-walk noise is actually quite low, namely only $\sim 4\ \mu\text{rad}/\sqrt{\text{Hz}}$. Similarly, the bias is comparatively low even for long coherence lengths ($\sim 30\ \mu\text{rad}$), although it is still too high for more demanding applications, as discussed later. This value is considerably lower than the early prediction of 35 mrad [1].

Fig. 4 points, for the first time, to two possible regimes of operation for laser-driven FOGs, each with several distinct potential advantages. The first is the region shown in the left-hand portion of the plots: using highly coherent, very narrow linewidth lasers. The two curves predict that lasers with linewidths falling in this region will exhibit extremely low ARW noise, much lower than that of a typical broadband source (typically $\sim\ 1\ \mu\text{rad}/\sqrt{\text{Hz}}$), but a fairly large drift. Applications requiring extremely high accuracy for short periods of time would benefit from this regime. Alternatively, by using a laser with a linewidth in the right-hand region of the plots in Fig. 4, both low noise and low drift can be achieved. For example, using a standard off-the-shelf telecom laser with a linewidth in the range of 10–100 MHz, the noise drops below that of a FOG operated with a broadband source while simultaneously achieving low drift. Drift levels in this right-hand region can meet typical requirements for inertial navigation ($\leq\sim 0.1\ \mu\text{rad}$). This combination of low noise and low drift comes with the important advantage that the center wavelengths of these lasers can be stabilized below the 1-ppm level, which again implies a good scale-factor stability.

Note that the modeling in Fig. 4 assumes a single-frequency laser. Sources with linewidths larger than ~100 MHz are generally not single frequency, and the analysis presented here would no longer be applicable. For example, a typical broad spectrum source, such as a superluminescent diode (SLD), oscillates at many different frequencies simultaneously. As a result, the assumed Wiener-Levy statistics of source phase noise in (12) would no longer be applicable. Indeed, the beating of these various frequencies results in source excess noise that increases rather than decreases with source linewidth. Evaluating the noise for linewidths significantly larger than the highest value shown in Fig. 4(a) (100 MHz) would therefore require including statistics to cover errors such as excess noise, which is not a trivial mathematical task.

B. Impact of Coupling Coefficient

Early investigations of coherent backscattering in FOGs predicted a strong dependence of the backscattering noise on the loop coupling coefficients in the case of very short coherence lengths [12]. Because backscattered light suffers a $\pi/2$ phase shift relative to the primary signal, when the coupling coefficients are exactly 0.5, for an unbiased FOG it can be shown that the backscattered signal is mostly in quadrature with the primary signal (limited only by the source coherence), and therefore the two signals do not interfere [12]. The result is a strong cancellation of the backscattering noise as the loop coupling coefficients approach 0.5.

For a sinusoidally biased FOG, the phase modulator has the potential to destroy the correlation between the scattered and primary fields because these fields arrive at the modulators at different times. Mackintosh *et al.* showed, however, that the correlation could be maintained if the FOG uses a single phase modulator operated at the loop proper frequency f_m and a short coherence length (<1 mm) [12]. All coherent scatterers are then very close to the loop midpoint, and because the phase is modulated at the loop proper frequency the scattered fields remain in quadrature with the primary fields. However, for longer coherence lengths this correlation is destroyed, potentially leading to an increase in backscattering-induced errors.

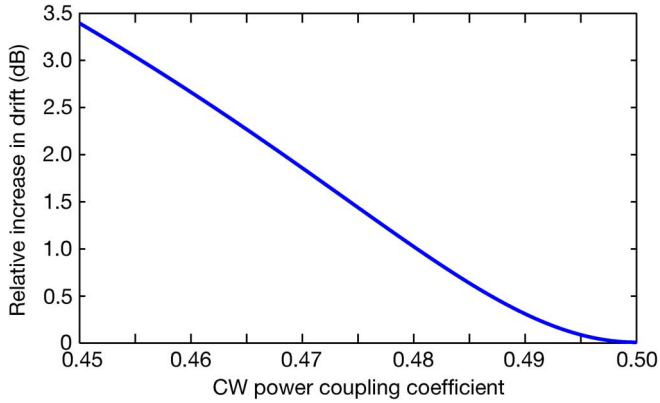

Fig. 5. Dependence of backscattering-induced drift on the loop coupling coefficient for a source with a 10-MHz linewidth.

An important contribution of this work is to show that by biasing a FOG with push-pull modulators, the requisite phase relation between scattered and primary fields can be restored for much longer coherence lengths. By operating the modulators at f_m and in opposite phase, an ideal 50% coupler again leads to cancellation of the backscattered signal, for any L_c. However, rather than the primary and scattered fields being directly in quadrature, the signal resulting from the interference between them is *modulated* in quadrature with the primary signals. Therefore, with a typical phase-sensitive detection the backscattering-induced error can be separated from the primary signal. In fact, for a perfectly coherent source and a symmetric coupler, no error is expected. For a finite linewidth of 10 MHz, Fig. 5 shows that deviation from the ideal coupler will lead to an increase in the bias drift: it more than doubles as the coupling coefficient goes from 0.5 to 0.45. Thus, even for longer coherence lengths, symmetric coupling and operation at the proper frequency lowers the backscattering error.

C. Impact of Fiber Loss

Loss in the fiber coil can also reduce the symmetry between scattered waves that is necessary for the above cancellation to occur. Referring to Fig. 2, when the scattering center is not located at the midpoint, the backscattered fields E_+^b and E_-^b traverse different optical paths. Combined with the fiber's finite loss, this path mismatch results in a different scattering amplitude upon exiting the coil, regardless of the symmetry of the loop coupler. The result is that loss reduces the symmetry between scattered fields and results in a larger expected drift.

This increase in drift, however, is highly dependent on the source coherence: for long coherence lengths, the solid curve in Fig. 6 shows that increasing the loss from 0.2 dB/km to 0.5 dB/km increases the drift by more than 2 dB. However, for

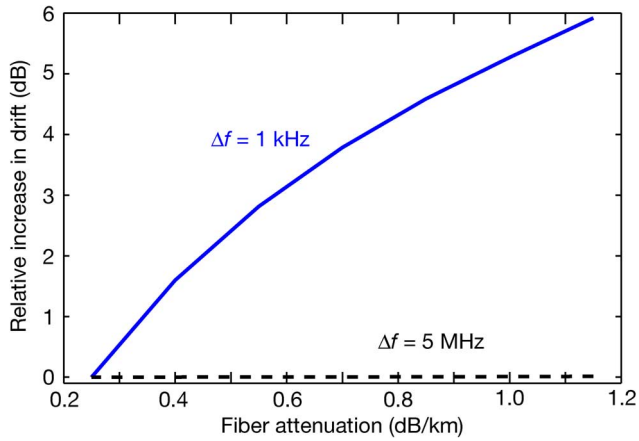

Fig. 6. Dependence of backscattering-induced drift on fiber loss, for two laser linewidths.

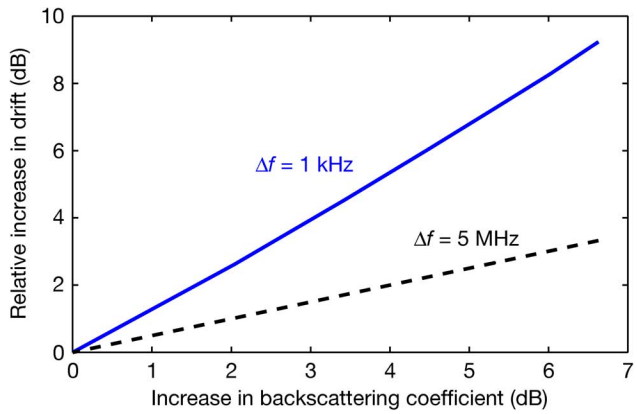

Fig. 7. Calculated increase in drift due to an increase in backscattering coefficient for two laser linewidths.

a shorter coherence length (dashed curve), increasing the loss has almost no effect over the loss range shown. For the relatively short coherence length of this 5-MHz source ($L_c \approx 13$ m in the fiber), the losses accrued over the portion of fiber that contributes to coherent backscattering are minimal, so the symmetry is maintained. Broader linewidth sources are much more tolerant to fiber losses, while greater care must be taken in selecting low-loss fiber when using a narrow-linewidth source.

D. Impact of Backscattering Coefficient

Fig. 7 shows the calculated dependence of the bias error on the backscattering coefficient α_B for two laser linewidths. These simulations assume that the loss is dominated by backscattering, i.e., that the fiber loss coefficient scales proportionally to α_B [19]. This may not be valid when comparing different types of fibers. In such cases, however, the analytical solution makes it straightforward to predict the drift given both the backscattering and loss coefficients.

Fig. 7 shows that for the 5-MHz laser (dashed curve) the drift increases with increasing backscattering coefficient as $\sim \sqrt{\alpha_B}$. When the linewidth is reduced to 1 kHz, the dependence on α_B is more rapid. In other words, increasing the backscattering coefficient has a significant effect on the observed drift for high-coherence lasers, but a smaller effect for low-coherence lasers. The reason is that as the α_B increases, the loss also does, and as explained in relation to Fig. 6, the drift increases more rapidly with increasing loss for a longer coherence laser.

Modeling also shows that the noise scales proportionally to $\sqrt{\alpha_B}$, independently of the laser coherence. For loop lengths shorter than L_c, we also found that the random-walk noise scales approximately as $L^{3/2}$. Since the FOG signal scales as $Le^{-\alpha L}$, [6] this result suggests that when $L_c \gg L$, shorter lengths give an improved signal-to-noise ratio (SNR), both in terms of bias error and noise. This is a different trend than either in the shot-noise-limited regime, where there is in fact an optimum coil length (generally several km), or in the excess-noise-limited regime, where noise and signal scale with length the same way and thus the SNR is independent of length.

When $L_c \ll L$, all backscattering-induced errors arise from the same portion of fiber centered at the loop midpoint. This implies that increasing the loop length will not lead to an increase in these errors. Instead, both the noise and drift are reduced due to the increasing propagation loss, while the rotation-induced signal increases as $Le^{-\alpha L}$. Therefore, in this regime, longer coil lengths improve the SNR. While this assertion is somewhat complicated by the changing modulation frequency, which affects the backscattering errors in complicated ways as explained above, it nevertheless remains valid. This is an important factor for ultimately building inertial navigation-grade FOGs driven with a laser, which require large scale factors, generally achieved by increasing the loop length.

V. Conclusions

We have presented the first quantitative analysis of the effect of coherent backscattering in the standard, minimum-configuration FOG driven with a light source of arbitrary coherence. Using analytic and numerical tools, this study points to several new important observations. First, the backscattering-induced noise can be made arbitrarily small by choosing either a very short coherence length, as previously applied with broadband light sources, or a coherence length very long compared to the loop length. This second regime of operation has not been demonstrated before and has important implications for developing FOGs with high scale-factor stability. Second, the long-term drift due to backscattering increases with increasing coherence length, up to an asymptotic value reached approximately when the coherence length equals the loop length. Even in the asymptotic range, where it is maximum, the drift is about 100 times smaller than roughly estimated in the past. For high-coherence sources this drift can be reduced by careful control of the loop coupler and phase modulation frequency. Third, this analysis points to a new mode of operation, which is to interrogate the gyro with a laser of modest coherence, namely with a coherence length shorter than the loop length yet significantly longer than the coherence length of a broadband source. In this regime, the noise can be below the excess noise of a broadband source, while the long-term drift approaches the level required for inertial-grade devices. Some techniques can be applied to reduce this drift further, including frequency modulation of the laser. Importantly, this performance comes with the overwhelming and unique advantage of a high scale-factor stability thanks to the highly stable frequency of a laser. Studies of the next

most significant source of noise and drift in a laser-driven FOG, namely polarization non-reciprocities, are needed in order to complete this prediction.

REFERENCES

[1] C. C. Cutler, S. A. Newton, and H. J. Shaw, "Limitation of rotation sensing by scattering," *Opt. Lett.*, vol. 5, no. 11, pp. 488–490, 1980.

[2] R. A. Bergh, B. Culshaw, C. C. Cutler, H. C. Lefèvre, and H. C. Shaw, "Source statistics and the Kerr effect in fiber-optic gyroscopes," *Opt. Lett.*, vol. 7, no. 11, pp. 563–565, 1982.

[3] G. A. Pavlath and H. J. Shaw, "Birefringence and polarization effects in fiber gyroscopes," *Appl. Opt.*, vol. 21, no. 10, pp. 1752–1757, 1982.

[4] G. A. Pavlath, "Fiber optic gyros: The vision realized," in *Proc. SPIE*, Aug. 2006, vol. 6314, Photorefractive Fiber and Crystal Devices: Materials, Optical Properties, and Applications XII, 63140G.

[5] H. Lefèvre, "Ultimate-performance fiber-optic gyroscope: A reality," presented at the 16th Opto-Electr. Commun. Conf., Kaohsiung, Taiwan, Jul. 2011.

[6] H. Lefèvre, *The Fiber-optic Gyroscope*. Norwood, MA, USA: Artech House, 1993.

[7] R. A. Bergh, H. C. Lefèvre, and H. J. Shaw, "An overview of fiber-optic gyroscopes," *J. Lightw. Technol.*, vol. 2, no. 2, pp. 91–107, Apr. 1984.

[8] H. G. Park, M. J. F. Digonnet, and G. S. Kino, "Er-doped superfluorescent fiber source with a ± 0.5 ppm long-term mean-wavelength stability," *J. Lightw. Technol.*, vol. 21, no. 12, pp. 3427–3433, Dec. 2003.

[9] S. Sunada, S. Tamura, K. Inagaki, and T. Harayama, "Ring-laser gyroscope without the lock-in phenomenon," *Phys. Rev. A*, vol. 78, pp. 053822-1–053822-8, 2008.

[10] K. Iwatsuki, K. Hotate, and M. Higashiguchi, "Effect of Rayleigh backscattering in an optical passive ring-resonator gyro," *Appl. Opt.*, vol. 23, no. 21, pp. 3916–3924, 1984.

[11] K. Takada, "Calculation of Rayleigh backscattering noise in fiber-optic gyroscospes," *J. Opt. Soc. Amer. A*, vol. 2, no. 6, June 1985.

[12] J. Mackintosh and B. Culshaw, "Analysis and observation of coupling ratio dependence of Rayleigh backscattering noise in a fiber optic gyroscope," *J. Lightw. Technol.*, vol. 7, no. 9, pp. 1323–1328, 1989.

[13] K. Krakenes and K. Blotekjaer, "Effect of laser phase noise in Sagnac interferometers," *J. Lightw. Technol.*, vol. 11, no. 4, pp. 643–653, 1993.

[14] P. Healey, "Statistics of Rayleigh backscatter from a single-mode fiber," *IEEE Trans. Commun.*, vol. 35, no. 2, pp. 210–214, 1987.

[15] P. Gysel and R. K. Staubli, "Statistical properties of Rayleigh backscattering in single-mode fibers," *J. Lightw. Technol.*, vol. 8, no. 4, pp. 561–567, 1991.

[16] S. W. Lloyd, "Improving Fiber Gyroscope Performance Using a Single-Frequency Laser," Ph.D. Dissertation, Appl. Phys. Dept., Stanford Univ., Stanford, CA, USA, 2012.

[17] N. J. Frigo, "Compensation of linear sources of non-reciprocity in Sagnac interferometers," in *Proc. SPIE*, 1983, vol. 412, pp. 268–271.

[18] B. Moslehi, "Analysis of optical phase noise in fiber-optic systems employing a laser source with arbitrary coherence time," *J. Lightwave Technol.*, vol. 4, no. 9, pp. 1334–1351, 1986.

[19] E. Brinkmeyer, "Analysis of the backscattering method for single-mode optical fibers," *J. Opt. Soc. Amer.*, vol. 70, no. 8, pp. 1010–1012, 1980.

Author biographies not included by author request due to space constraints.